

Magnetic Properties of Fe²⁺-Doped MnCO₃[†]

I. Maartense

Department of Physics, University of Manitoba, Winnipeg 19, Canada

(Received 29 October 1971)

Magnetization and susceptibility measurements have been made on pure and Fe²⁺-doped MnCO₃ powders of ~0.5-μm particle size. Through the disappearance of weak ferromagnetism, the Mn²⁺ spin system is seen to be reoriented from the basal plane to the trigonal axis as the Fe content is increased. Zn doping has no such effect. The reorientation is thought to be caused by the large uniaxial anisotropy of the Fe²⁺ ground-state spins, with the Mn spin direction being determined mainly by competition between Mn-Fe exchange and the relatively small magnetic dipolar anisotropy of Mn favoring the basal plane. The remanent weak moment decreases rapidly above a critical concentration of 0.5 at. % Fe, to about $\frac{1}{10}$ of the undoped value for 2 at. %. For higher dopings, the materials behave as uniaxial antiferromagnets at low fields, but their nonlinear susceptibility shows that spin rotation in an external field returns the Mn sublattices toward the basal plane; a critical field of ~25 kOe is inferred from the data for 5 at. % Fe. In the transition doping range, a large thermoremanent offset moment results in shifted hysteresis loops of the normal weak moment. This offset, amounting to a maximum of ~1.5 μ_B per Fe²⁺ ion at a doping level of 0.9 at. %, is attributed to stabilization of the Fe²⁺ polarization, induced near T_N , by an exchange barrier arising out of a non-collinear Mn-Fe spin arrangement. Below the critical concentration, the near absence of an offset moment implies that the Mn and Fe spins are either almost parallel or almost perpendicular to each other. By considering a simple model, the latter is taken to be the most probable situation. At the upper end of the transition range (~2 at. % Fe), $\chi_0(T)$ shows a weak ferromagnetic-to-antiferromagnetic transition near $T_N - 1^\circ\text{K}$. The variation of T_N with doping is nonlinear, T_N being 34.5, 35, and 38°K for 0, 5, and 20 at. % Fe²⁺, whereas the reported value for FeCO₃ is 38.3°K. Also pointed out is the probability of occurrence of a photomagnetic effect, in this and similar systems, through an effective reduction in the doping concentration by excitation of the impurity ions.

INTRODUCTION

Solid solutions of FeCO₃ in MnCO₃ have interesting magnetic properties because of the differing characteristics of their constituents. Although both materials have exchange interactions which lead to antiferromagnetic ordering near $T_N \approx 35^\circ\text{K}$, the anisotropy energies which define the easy directions of the ordered spins in these rhombohedral crystals have different origins and this results in large differences in their magnetic behavior. In the S-state ion Mn²⁺, a relatively weak anisotropy, favoring spin directions in the basal plane, is the result of the long-range magnetic-dipolar interactions.^{1,2} In FeCO₃, the Fe²⁺ spins are tightly bound to the trigonal-*c*-axis direction by a large anisotropy energy arising out of the action of the crystalline electric field and spin-orbit coupling on the ⁵D ground state.^{3,4} When Fe²⁺ is substituted for Mn²⁺, there will be a loss of exchange energy if the Mn²⁺ and Fe²⁺ spins remain noncollinear. Consequently, a balancing of the exchange and anisotropy energies will result in rotations of the spins away from their easy directions. Owing to the relatively large Fe²⁺ anisotropy, only a small iron concentration is required to reorient the Mn sublattices from the basal plane to the *c* axis.

The main reason for the experimental interest in this system is the presence of weak ferromagnetism. The magnetic symmetry of these materials allows an antisymmetric exchange interaction of the form $\vec{D} \cdot (\vec{S}_1 \times \vec{S}_2)$, with the vector \vec{D} parallel to the trigonal axis.⁵ Thus a mutual canting of the sublattices containing spins \vec{S}_1 and \vec{S}_2 occurs through this interaction only when there are spin components in the basal plane. The resulting net moment in this plane then acts as a convenient handle on the spin system whereby its average orientation can be found through magnetization measurements, even in powdered samples.

It has previously been shown⁶ that weak ferromagnetism is absent in a natural MnCO₃ crystal containing 5 at. % Fe, and that the spins are parallel to the trigonal crystal axis. This paper is concerned mostly with the Fe-concentration dependence of the macroscopic magnetic properties of doped MnCO₃ powders. The orientation of the Fe²⁺ impurity spins can be determined at the microscopic level by means of the Mössbauer effect; this work is in progress and will be published at a later date.⁷

EXPERIMENTAL RESULTS

FeCO₃ and MnCO₃ have the same rhombohedral crystal structure with similar lattice constants,

so that Fe²⁺ is readily substituted for Mn²⁺. The iron-doped samples were prepared from aqueous solutions of MnSO₄ and FeSO₄, in the desired ratio, by precipitating the carbonate in a quartz test tube by adding NaHCO₃ powder. The tube with the reaction products was then heated in a sealed vessel for about 24 h at 200 °C, to increase the particle size. The recrystallized material was washed in water and acetone and dried. The color of the powders is pale pink at low doping levels, tending toward light cream as the iron concentration is increased. The material has been stable in air for at least two years, as shown by a comparison of old and fresh powders. The lattice parameters vary smoothly with Fe content, while there is no change in the x-ray-diffraction linewidths. This contrasts with zinc-doped MnCO₃, prepared in a similar fashion, which shows distinct line broadening, as well as the presence of different phases for some high Zn concentrations.

Electron micrographs reveal particles in the form of platelets with rhombohedral faces, whose large dimensions are about 0.5 μm, rather than the expected hexagonal plates with faces parallel to the basal plane.⁸ Magnetization measurements on wax-embedded powders were performed with a vibrating sample magnetometer, while the variation of the initial susceptibility with temperature was obtained with an rf magnetometer⁹ operating at 10 MHz.

The magnetic-moment data, some of which are drawn in Fig. 1, show the decrease in the weak moment as the Fe-doping level is increased. A coercive force H_c can here be defined as the field at which a hysteresis loop crosses a line representing the induced antiferromagnetic moment $M = \chi_a H$, rather than the $M = 0$ axis, where χ_a is

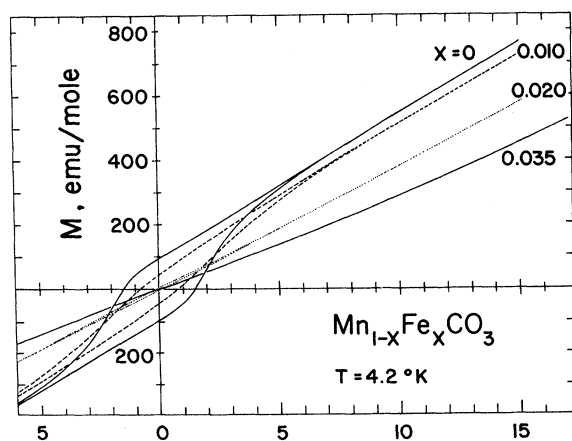


FIG. 1. Hysteresis loops of some Fe²⁺-doped MnCO₃ powders of ~0.5-μm particle size, at 4.2 °K.

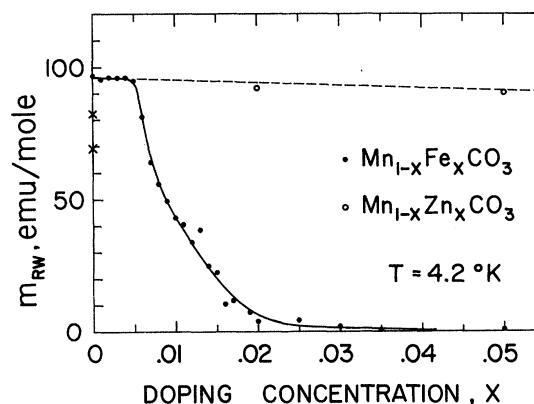


FIG. 2. The remanent moment per mole of sample, at 4.2 °K, of Fe²⁺- and Zn²⁺-doped MnCO₃ powders. The broken line denotes a constant moment per mole of MnCO₃. Particle size is ~0.5 μm except for the two data points on $x=0$ axis which represent smaller particles; see text.

the antiferromagnetic susceptibility obtained from the slope of a loop's descending branch near saturation of the weak moment. The coercive force of all samples of this particle size is found to be about 2 kOe. The changing nature of the non-linearity of the descending branches of the hysteresis loops makes comparison of the zero-field extrapolated moments of the samples worthless; however, the powder remanent moment is expected to be a fixed fraction of the saturated weak moment in these single-domain particles (see below), and therefore should be a reliable indicator of the weak moment. Figure 2 shows the remanent weak moment, $m_{RW}(x)$, at 4.2 °K, as a function of the molar Fe concentration x ; m_{RW} is defined as the moment where a hysteresis loop crosses the $H = 0$ axis. The moment begins to decrease abruptly near $x = 0.005$, and is less than $0.1m_{RW}(0)$ for $x = 0.02$. That the disappearance of the weak ferromagnetism is associated with magnetic interactions with the Fe²⁺ impurities is proved by the persistence of the weak moment in samples doped with diamagnetic Zn²⁺. In that case, the moment of the MnCO₃ molar fraction remains nearly constant (broken line in Fig. 2). It could be argued that this is the result of mixing of separated MnCO₃ and ZnCO₃ phases, but a depression of the Néel point, which is also observed, is not consistent with that interpretation.

The saturated weak moment, extrapolated to $H = 0$, of a natural crystal containing little or no Fe (as shown by optical fluorescence, see Conclusions) is found to be 186 ± 2 emu/mole at 4.2 °K, agreeing with Borovik-Romanov's result.¹⁰ Thus the remanent moment of 0.5-μm particles of pure MnCO₃ powder (96 emu/mole, Fig. 2) represents ~52% of the saturated moment. Also shown on the

$x = 0$ axis are the remanent moments of smaller powder particles. The lowest value corresponds to $\sim 0.02\text{-}\mu\text{m}$ size.⁶ The intermediate value is the remanence of MnCO_3 precipitated at room temperature and not recrystallized at a higher temperature; its particle size was not measured. For comparison, a sample of coarse MnCO_3 crushed to $\sim 2\text{-}\mu\text{m}$ particles was found to have a remanence only slightly larger than that of the $0.5\text{-}\mu\text{m}$ powder used in the rest of this investigation, which can then be taken as typical single-domain material. The remanence ratio decreases again in particles larger than $\sim 20\text{ }\mu\text{m}$, presumably due to the formation of domain walls.

The nonlinear magnetization $M(H)$, seen in Fig. 1, is most easily interpreted in terms of the differential susceptibility $\chi(H) = dM(H)/dH$, as plotted in Fig. 3. The high-field susceptibility of pure MnCO_3 represents the transverse susceptibility, χ_{\perp} , of the Mn^{2+} spins, these spins being always perpendicular to the measuring field because of the small basal-plane anisotropy; thus, $\chi_{\perp} = 43 \times 10^{-3}$ emu/mole Oe. The low-field behavior is dominated by the magnetization process of the weak moment, for small x . However, for $x > 0.02$, the low-field χ has dropped to $\sim \frac{2}{3} \chi_{\perp}$, the powder susceptibility expected of a magnetically uniaxial material. This is convincing evidence of the change of orientation of the Mn^{2+} spins towards the tri-

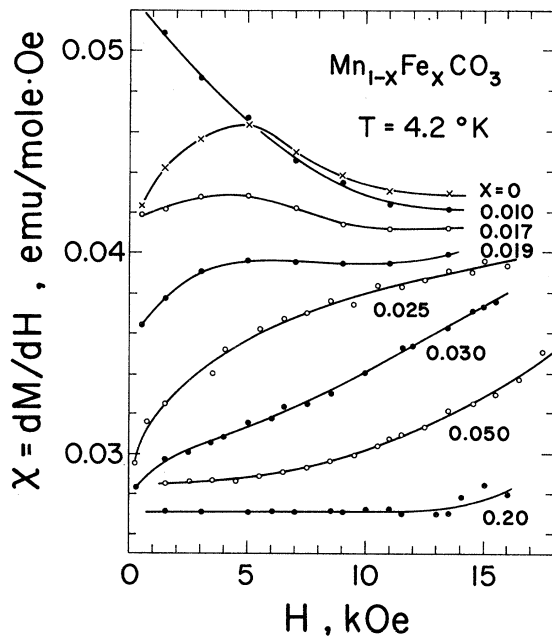


FIG. 3. Differential susceptibility of Fe^{2+} -doped MnCO_3 powders at $4.2\text{ }^\circ\text{K}$. The four uppermost curves correspond to the descending branches of the hysteresis loops; the remaining curves include points for both increasing and decreasing H .

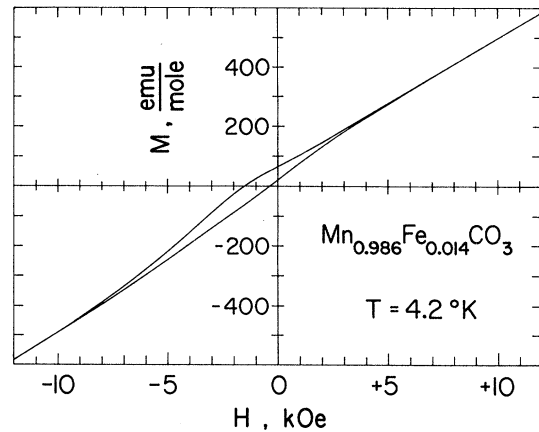


FIG. 4. Typical offset hysteresis loop at $4.2\text{ }^\circ\text{K}$; MnCO_3 powder doped with 1.4 at. % Fe, cooled through T_N in $+15\text{ kOe}$.

gonal axis. As x is increased further, χ continues to decrease because of the relatively low susceptibility of the Fe^{2+} ions, as in FeCO_3 powder.¹¹ As the applied field is increased, $\chi(H)$ for $x > 0.02$ begins to return to a value equivalent to χ_{\perp} . This behavior is evidently caused by rotation of the Mn^{2+} spins back toward the basal plane; the field required for this rotation, which appears to be less than 1 kOe for $x = 0.02$, is then seen to increase rapidly with Fe content.

For $x < 0.02$, the presence of hysteresis makes $\chi(H)$ asymmetrical, with the usual maximum near the reverse field value corresponding to the average coercive force, as the moment is reversed. In Fig. 3, therefore, only the descending branches are plotted for these concentrations. In pure MnCO_3 , $\chi(H)$ decreases towards low fields; this decrease was observed more clearly in $\sim 0.02\text{-}\mu\text{m}$ particles, with $H_c \approx 4\text{ kOe}$, where it was associated⁶ with a magnetization process involving spin flopping of the sublattices within the basal plane.

When samples in the transition doping range, $0.005 < x < 0.03$, are cooled through T_N in an external field, a very hard thermoremanent moment results. This leads to hysteresis loops which are offset on the moment axis and are shifted by 0.5–1 kOe on the reverse field axis; a typical loop is shown in Fig. 4. The value of the remanent weak moment, m_{RW}^0 , taken to be half the width of the offset loop on the M axis, and its coercive force are almost unchanged from the normal loop, while the offset moment itself has a very high coercive force ($> 15\text{ kOe}$; i. e., the offset remains after cycling the sample in an applied field of $\pm 15\text{ kOe}$ at $4.2\text{ }^\circ\text{K}$).

The thermoremanent offset moment, m_{RO} , defined as the midpoint on the M axis of the offset hysteresis loop, is plotted as a function of doping concentration in Fig. 5(a). Taking m_{RO} to be

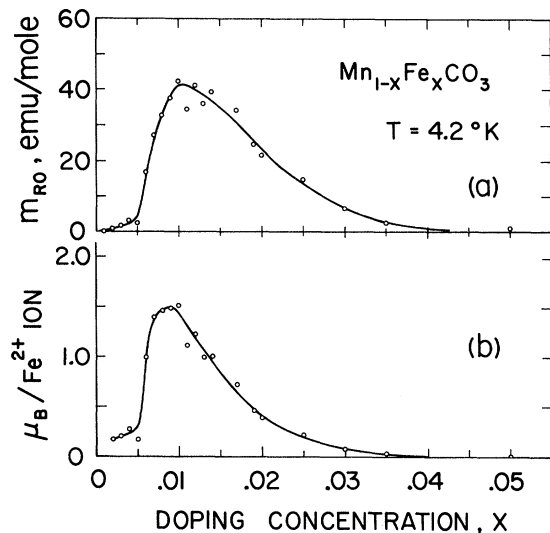


FIG. 5. Remanent offset moment, at 4.2°K, of Fe^{2+} -doped MnCO_3 powders cooled through T_N in 15 kOe; (a) per mole of sample; (b) average effective number of Bohr magnetons per Fe^{2+} impurity ion.

aligned along some easy direction, so that a powder remanence ratio of $\frac{1}{2}$ is applicable, and assuming that the offset moment is associated with the impurities, the average polarization per Fe^{2+} ion is shown in Fig. 5(b). An offset can be produced only within the doping region where the weak moment disappears (Fig. 2); above a "critical concentration" $x \approx 0.005$, m_{RO} rises quickly to $\sim 1.5 \mu_B$ per Fe^{2+} ion.

Figure 6 shows the temperature variation of the remanent moments, m_{RW} and $(m_{RW}^0 + m_{RO})$, obtained by warming previously saturated samples in zero external field. In the former case [Fig. 6(a)], the samples were cooled in zero field before saturation; the latter quantity [Fig. 6(b)] is the total thermoremanent moment of samples cooled to 4.2°K in 15 kOe. In general, the offset moment falls more rapidly than the sublattice magnetization, as represented by the weak moment, m_{RW} , of pure MnCO_3 . The change in critical behavior from that of a weak ferromagnet to that of a uniaxial antiferromagnet is most clearly seen in Fig. 7, where the initial susceptibility, $\chi_0(T)$, at 10 MHz is recorded for a wide range of Fe concentrations.

DISCUSSION

The limiting of the remanence ratio of the weak moment at $\sim \frac{1}{2}$ in MnCO_3 powder is surprising, for a material which is expected to have an easy plane of magnetization with three equivalent easy axes and hence a ratio of $\frac{3}{4}$.¹² The observed remanence ratio of $\frac{1}{2}$ implies that only one easy axis exists in the basal plane of the powder particles. This cannot be caused by shape anisotropy, in the

usual sense,¹³ since the demagnetizing fields in the basal plane can amount to no more than about 40 Oe; this value is too small to have a measurable effect in samples which have a coercive force of ~ 2 kOe (Fig. 1). A plausible explanation of the uniaxial behavior is that differential thermal contraction of the platelike rhombohedral crystallites leads to anisotropic stresses within the particles. Through magnetostriction, stress-induced anisotropy fields of the order of 1 Oe can then arise in the basal plane.¹⁴ Such fields can dominate¹⁴ the basal-plane anisotropy H'_A and can thus define a unique easy axis by means of the spin-flop magnetization process.⁶ The coercive force is then determined by the in-plane spin-flop field $(2H'_A H_E)^{1/2}$, where H_E is the exchange field; in this way an effective "shape-induced stress anisotropy" of the order of 1 kOe can result. Only in powders of crystallites formed as hexagonal prisms on the trigonal crystal axis should the remanence ratio attain the value $\frac{3}{4}$.

The decrease in the remanent moment of very

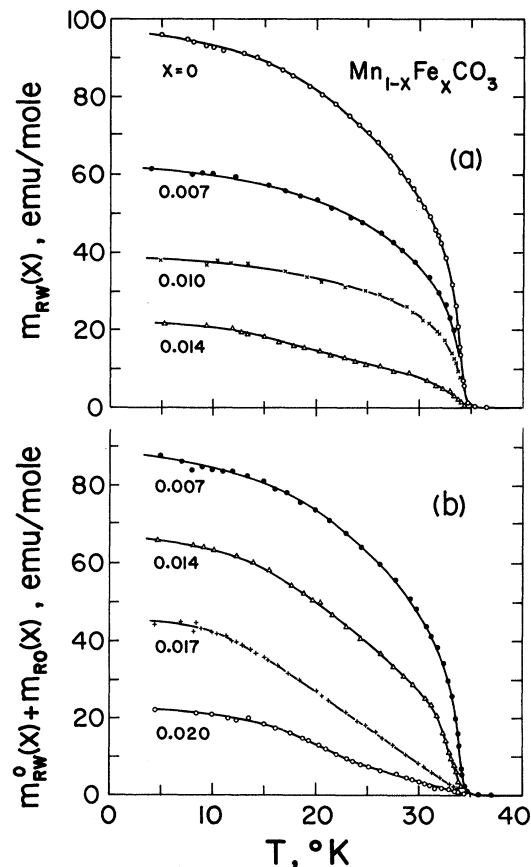


FIG. 6. Remanent moments as a function of temperature for Fe^{2+} -doped MnCO_3 powders; (a) normal remanence (samples cooled in zero field, then saturated); (b) sum of normal and offset remanences (samples cooled in 15 kOe).

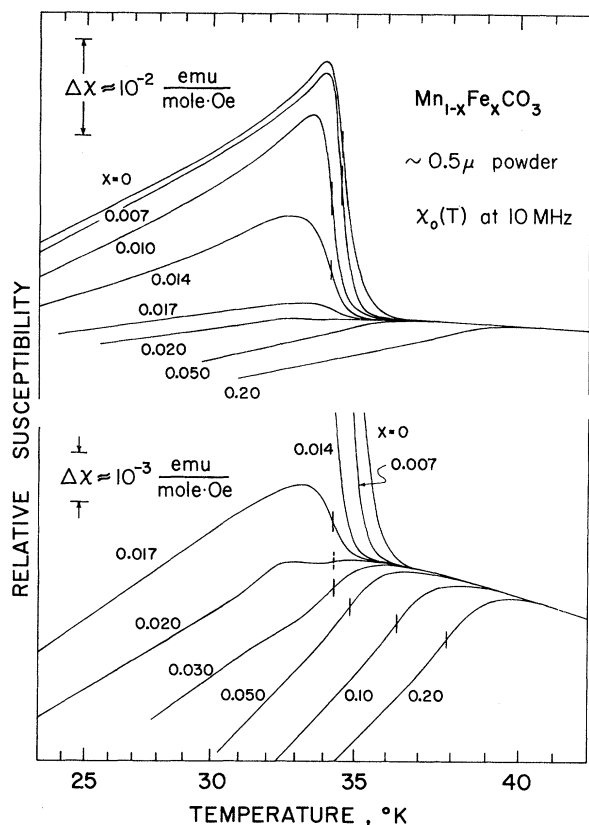


FIG. 7. Initial rf susceptibility near the ordering temperatures of Fe^{2+} -doped MnCO_3 powders. The recorder tracings have been fitted to a common asymptote above T_N ; the experimental definitions of T_N are marked on the curves by vertical lines.

fine powders ($x = 0$, Fig. 2) is not caused by a remanence ratio which is less than $\frac{1}{2}$, but rather by a true decline in the weak moment as the particle surface-to-volume ratio is increased. This statement is supported by the $\sim 2^\circ\text{K}$ difference in the ordering temperatures of 0.02- and 0.5- μm powders.¹⁵

The basic interpretation of the iron-concentration dependence of the saturation value of the spontaneous weak moment, $m_w(x)$, remains simple. In the Fe-doping range $x = 0$ to $x \approx 0.005$ the Mn^{2+} spins lie in, or close to, the basal plane so that $m_w(x)$ is nearly constant. In the transition range $x \approx 0.005$ – 0.03 , a competition between anisotropy and exchange interactions of Mn^{2+} and Fe^{2+} results in a rapid change of the average equilibrium orientation of the Mn spin system from the basal plane to the c axis, with an attendant decrease in $m_w(x)$. With higher Fe doping, the spins are nominally parallel to the c axis, the easy direction of the Fe^{2+} spins, and $m_w(x) \rightarrow 0$.

Taking the remanence ratio $m_{\text{RW}}(x)/m_w(x)$ to be independent of x , the angle θ_{Mn} between the Mn^{2+}

spin axis and the crystal c axis can be deduced from the measured values of $m_{\text{RW}}(x)$, at 4.2°K . If the total weak moment originates from the antisymmetric exchange interaction of the Mn^{2+} sublattices, then the canting angle ϕ_0 of the spin components in the basal plane [see Fig. 8(a)] is to a first approximation independent of θ_{Mn} . This is easily seen by minimizing the exchange energy within the Mn^{2+} system,

$$E_{\text{ex}} = J\vec{S}_1 \cdot \vec{S}_2 - \vec{D} \cdot (\vec{S}_1 \times \vec{S}_2),$$

for a given value of θ_{Mn} , and making the reasonable assumption that the ratio of the exchange parameters D/J is independent of θ_{Mn} . Then

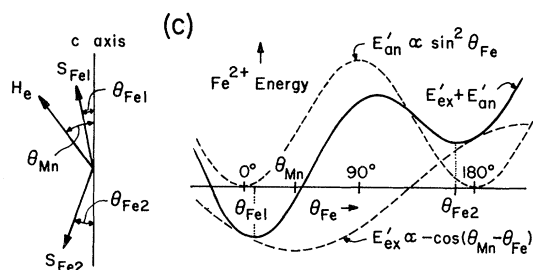
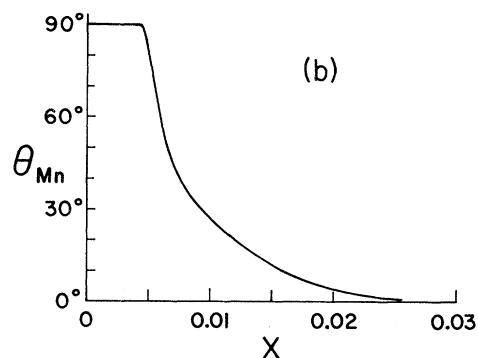
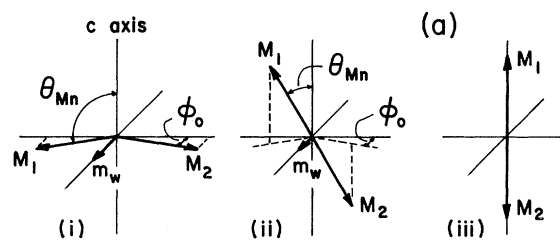


FIG. 8. (a) Model of the Mn^{2+} sublattice orientations in (i) pure MnCO_3 , and in Fe^{2+} -doped MnCO_3 in (ii) the transition-doping range and (iii) the highly doped range ($x > 0.03$); m_w is the resultant weak moment in the basal plane. (b) Angular variation of the Mn^{2+} spin direction as deduced from the data in Fig. 2. (c) Model of the Fe^{2+} spin directions, illustrating the existence of a second metastable orientation, used to explain the presence of a thermoremanent offset moment.

$$\sin\theta_{\text{Mn}} = m_{\text{W}}(x)/m'_{\text{W}}(x) = m_{\text{RW}}(x)/m'_{\text{RW}}(x),$$

where $m'_{\text{W}}(x)$ and $m'_{\text{RW}}(x)$ are the moments of the equivalent molar fraction of pure MnCO₃ at the doping concentration x [the broken line in Fig. 2 is $m'_{\text{RW}}(x) = (1-x)m_{\text{RW}}(0)$]. A plot of $\theta_{\text{Mn}}(x)$ made in this way from the data in Fig. 2 is shown in Fig. 8(b). The value of θ_{Mn} for $x < 0.005$ is drawn as 90° although the slow variation of $\sin\theta_{\text{Mn}}$ near 90°, together with the experimental scatter in the data, allows values of θ_{Mn} down to about 80°. At the higher doping levels, θ_{Mn} will be underestimated if the weak moment changes sign or direction within individual particles due to the presence of the Fe impurities, so that the effective remanence ratio is reduced. Nevertheless, a rapid decrease in θ_{Mn} above $x \approx 0.005$ must be inferred from the measurements.

The deviations $\Delta\theta_{\text{Mn}}$ of individual spin directions from the average direction of the Mn²⁺ spin axis of each sublattice are taken to be small. This assumption is valid because the anisotropy forces acting on the Mn²⁺ spins are very small¹ (~1%) compared to the exchange forces, so that these spins will tend to couple collinearly in the space between Fe²⁺ impurities.

In the present model of the spin orientations, the angle θ_{Mn} is determined independently of Mn-Mn exchange coupling, by interaction of the entire Mn²⁺ spin system with the isolated Fe²⁺ impurity ions. A representation of the Mn²⁺ spin directions for the low-, intermediate-, and high-doping concentrations is shown in Fig. 8(a). A theoretical calculation of the equilibrium Mn and Fe spin angles as a function of doping, $\theta_{\text{Mn}}(x)$ and $\theta_{\text{Fe}}(x)$, will require more detailed information on the Mn-Fe exchange interactions and Fe²⁺ anisotropy than is presently available. However, it can be expected that, because of the large ratio of anisotropy to exchange energy of the Fe²⁺ ground-state spins,³ the Fe²⁺ moment will not necessarily be parallel to the Mn²⁺ spin system so that θ_{Fe} can be less than θ_{Mn} . Evidence of such noncollinearity is found in the offset moment which can be induced in the intermediate-doping range (Fig. 5). At present, these measurements supply the only information on the orientation $\theta_{\text{Fe}}(x)$ of the Fe²⁺ moment.

Since the offset cannot be established or reversed in an applied field of 15 kOe, at 4.2°K, it is not likely to be due to an isothermal magnetization process. Furthermore, its rapid decrease above $x = 0.01$ shows that the offset is not associated with nonrandom clusters of FeCO₃ with a net ferromagnetic moment.¹⁶ A reasonable explanation is that the polarization induced in the Fe²⁺ spins by the external field near the ordering temperature T_N is "frozen in" below T_N by a Mn-Fe exchange field

which is not collinear with the Fe²⁺ spin directions. This proposed origin of the offset moment can be understood with the aid of the basic model illustrated in Fig. 8(c). Using rather simple formulations for the orientation dependences of the Fe²⁺ anisotropy and exchange energies such that $E'_{\text{an}} \propto \sin^2\theta_{\text{Fe}}$ and $E'_{\text{ex}} \propto -\cos(\theta_{\text{Mn}} - \theta_{\text{Fe}})$, a secondary, metastable energy minimum occurs in $E'_{\text{an}} + E'_{\text{ex}}$ for sufficiently small $E'_{\text{ex}}/E'_{\text{an}}$. As long as a sample is not cooled in a field, the distribution of Fe²⁺ spins between the orientations $\theta_{\text{Fe}1}$ and $\theta_{\text{Fe}2}$ will be the same for both antiferromagnetic host sublattices, so that there will be no net Fe²⁺ moment. When an applied field induces a polarization in the paramagnetic ions above T_N , an unequal distribution of spins will be frozen in when long-range magnetic order sets in, resulting in an unbalanced Fe²⁺ moment. In the case of high Fe-doping concentrations ($x > 0.03$) where $\theta_{\text{Mn}} \approx \theta_{\text{Fe}} \approx 0$, the situation will be similar to that in metamagnetic⁴ FeCO₃ and the spin distributions will be rapidly equalized through the reversal of a number of spins. The fact that the offset moment is stable for $x < 0.03$ suggests that for the supposed spin arrangement with $\theta_{\text{Mn}} > \theta_{\text{Fe}} > 0$, where $\theta_{\text{Fe}1} \neq \theta_{\text{Fe}2}$, transitions between the two Fe²⁺ states have a low probability since more than a simple spin reversal of Fe²⁺ ions is involved. In a sense, the excess energy of the metastable Fe²⁺ state is shared by the surrounding host ions through the exchange coupling, and a change in θ_{Fe} must be accomplished by some readjustment of θ_{Mn} .

If the Fe²⁺ ground-state moment is taken to be $|\vec{2S} + \vec{L}| \approx 5\mu_B$,³ the net offset of $\sim 1.5\mu_B$ [at $x = 0.009$, Fig. 5(b)] represents about 30% of the completely polarized Fe²⁺ moment. The disappearance of the offset moment when $x < 0.005$ can have two causes. In the present model, a thermoremanent offset should be expected whenever $0 < (\theta_{\text{Mn}} - \theta_{\text{Fe}}) < 90^\circ$. At one limit, when $\theta_{\text{Mn}} = 90^\circ$ and $\theta_{\text{Fe}} = 0$, the impurity spins are perpendicular to the host sublattice and $E'_{\text{ex}} = 0$; the "up" and "down" states of Fe²⁺ become energetically indistinguishable and their populations will quickly equalize. At the other extreme, $\theta_{\text{Fe}} \rightarrow \theta_{\text{Mn}} \rightarrow 90^\circ$ and the metastable energy minimum sketched in Fig. 8(c) will disappear. The experimental data do not define which of these descriptions best fits the real material, although the model considered here favors the case with $\theta_{\text{Fe}} \rightarrow 0$, such that the Fe²⁺ spin component in the basal plane is small. However, the correct quantum-mechanical description of the Fe²⁺ anisotropy is more complicated than assumed here; indeed, Ok¹⁷ has interpreted Mössbauer data on Fe-doped CoCO₃ to show that $\theta_{\text{Fe}} \rightarrow 90^\circ$ in that system. A fuller treatment of the Fe²⁺ spin behavior in MnCO₃ will be published later.⁷

The differential susceptibility data in Fig. 3 should not be analyzed, at low doping levels, in terms of spin flopping alone, since a transverse-field-induced canting transition may also occur.¹⁸ The restoration of the weak moment, as the Mn spin directions return to the basal plane, probably determines the detailed shape of the dM/dH curves for $x < 0.02$ where the critical fields are expected to be low. In Fig. 3, only the data for $x = 0.05$ are amenable to simple analysis in terms of a quadratic field dependence of $\chi(H)$.¹⁹ An average uniaxial anisotropy constant $K \approx 1.2 \times 10^7$ erg/mole is found at 4.2 °K, for $x = 0.05$, corresponding to an effective average anisotropy field $H_A = K/M_0 \approx 900$ Oe, using $M_0 = 13\,950$ emu/mole. Thus the spin-flop field $\approx (2H_A H_E)^{1/2}$ should be ~ 25 kOe; earlier it was found⁶ that, in a single crystal with $x = 0.05$, the spin-flop field applied along the trigonal axis was greater than 13.5 kOe. If the average "anisotropy" is assumed to change sign in the transition region near $x = 0.01$, then $K(x)$ is seen to be a nonlinear function, since $|K(0)| = 4.1 \times 10^7$ erg/mole at 4.2 °K.²⁰ Of course, the present $K(x)$ is not a normal anisotropy since it is supposed to arise from exchange interactions. Even above the Fe concentration where all spins are aligned on the c axis, a nonlinear $K(x)$ is expected, owing to the increasing importance of Fe-Fe exchange. Above some concentration, the metamagnetic character of FeCO_3 ⁴ should become dominant over the spin-flop behavior of the Mn spins.

The change from weak ferromagnet to uniaxial antiferromagnet, shown by $\chi_0(T)$ in Fig. 7, confirms the Fe-doping dependence seen in more detail in Fig. 2. The variation of $T_N(x)$ in the transition region is difficult to measure in these fine powders,¹⁵ but appears to be small. T_N is defined by the inflection point in $\chi_0(T)$, as marked in Fig. 7. In the uniaxial region, above $x \approx 0.03$, T_N varies rapidly from 35 °K at $x = 0.05$ to 38 °K at $x = 0.20$. Since $T_N = 38.3$ °K in pure FeCO_3 ,²¹ $T_N(x)$ is nonlinear, apparently having a maximum at some value of $0 < x < 1$. The same situation occurs in Fe^{2+} -doped MnF_2 ,²² and is attributed to an increased strength of the ferromagnetic exchange between impurity and host within the same sublattice, as compared to the end members of the substitution series.

Evidence of a temperature-induced spin reorientation in a sample with fixed Fe concentration is supplied by the data for $x = 0.02$ in Fig. 7. The behavior at T_N is uniaxial, but at $\sim T_N - 1$ °K a maximum, characteristic of weak ferromagnetism, appears; a similar behavior is barely visible for $x = 0.03$ near $T_N - 2$ °K. Thus a reorientation occurs only at doping concentrations where the low-temperature weak moment has almost disappeared,

i. e., where $\theta_{\text{Mn}} \rightarrow 0$.

A weak ferromagnetic-to-uniaxial-antiferromagnetic transition with increasing temperature is not unexpected on the basis of the different temperature dependences of the Fe and Mn anisotropies. The Fe spin anisotropy should vary relatively slowly in the region of interest, since only the lowest electronic energy level is populated to any significant extent³; this also shows in the large anisotropy of the paramagnetic susceptibility above T_N .¹¹ The Mn anisotropy, on the other hand, will have a variation determined by the square of the sublattice magnetization because of its dipolar origin.²

CONCLUSIONS

The present results on Fe^{2+} -doped MnCO_3 powder give a fairly complete insight into the behavior of the Mn spin system as a function of impurity concentration. Above a critical Fe content of about 0.5 at.%, the loss of the weak ferromagnetic moment shows that a rapid reorientation from the basal plane to the trigonal axis takes place. The data also show that, above doping levels at which the axial alignment is nominally complete, the Mn spins can be rotated back to the basal plane in an external field. There is also evidence of a temperature-induced weak ferromagnetic-to-antiferromagnetic transition close to T_N for relatively highly doped samples (~ 2 at.% Fe).

There is no direct information on the Fe^{2+} spin directions at low doping concentrations, except that the presence of a thermoremanent offset moment shows that the Mn and Fe spins are noncollinear in the transition range of doping ($0.005 < x < 0.03$). Below the critical Fe concentration the data allow Fe^{2+} spin orientations which are either nearly parallel or perpendicular to the basal plane. It is expected that studies of the Mössbauer effect in ^{57}Fe -doped samples, presently in progress,⁷ will provide a more complete description of the Fe^{2+} spin behavior.

Some aspects of the proposed model of the spin orientations should be tested with measurements on single crystals. Only then, for instance, will orientation studies of the offset moment be possible; in addition, it will be possible to determine whether well-defined critical fields exist for Mn^{2+} spin flopping and other spin-reorienting processes.¹⁸

The possibility of an interesting photomagnetic effect exists in Fe^{2+} -doped MnCO_3 and similar systems. Because of the rapid change of the magnetic properties as the Fe concentration is changed, just above the critical concentration, even a small change in the number of Fe^{2+} electronic ground-state spins can be detected. If a sufficient population of one of the higher energy states of Fe^{2+} , with

a less anisotropic character; can be achieved for a time long enough to allow relaxation of the Mn²⁺ spins toward the basal plane, an effective decrease in the instantaneous impurity concentration will result. In other words, excitation of the Fe²⁺ ions should manifest itself through the Mn spin system, by an increase in the weak ferromagnetic moment, or a decrease in the spin-flop field, depending upon the actual doping level. In the latter case a single crystal, biased just below the critical field, would show spin flopping after excitation of the impurities. Alternately, excitation of the Fe ions could be detected directly by a "discharging" of a previously stored offset moment; this moment would be read out only once per charging cycle, assuming that the Fe spins will be randomized while in the excited states.

Some indication that the necessary excitation conditions are present is given by preliminary

fluorescence experiments. The typical red fluorescence of "pure" MnCO₃, when excited in the near-ultraviolet, is greatly enhanced in the Zn-doped samples. However, even a very small amount of Fe impurity is sufficient to quench the Mn fluorescence, probably because of the near resonance of states of the ⁴G and ³H manifolds of Mn²⁺ and Fe²⁺, especially in the 4000-Å region. The possibility exists that an appreciable excited-state population can be established in Fe²⁺ by pumping of the host MnCO₃.²³ The efficiency of this energy transfer will determine the heating load placed on the crystal lattice for a given change in the effective doping concentration. The way in which the excited-state energy is degraded to the ground state is the decisive factor in allowing a measurable photomagnetic effect; that is, a metastable Fe²⁺ state with a lifetime of the order of 10⁻³ sec or longer is desirable.

†Work supported by the National Research Council of Canada. A preliminary account was given at the CAP-APS-SMF Conference, Winnipeg, 1970; *Bull. Am. Phys. Soc.* **15**, 825 (1970).

¹H. J. Fink and D. Shaltiel, *Phys. Rev.* **130**, 627 (1963).

²B. Y. Kotyuzhanskii, *Zh. Eksperim. i Teor. Fiz.* **59**, 1562 (1970) [*Sov. Phys. JETP* **32**, 854 (1971)].

³J. Kanamori, *Progr. Theoret. Phys. (Kyoto)* **20**, 890 (1958).

⁴I. S. Jacobs, *J. Appl. Phys.* **34**, 1106 (1963).

⁵I. Dzyaloshinsky, *J. Phys. Chem. Solids* **4**, 241 (1958); T. Moriya, *Phys. Rev.* **120**, 91 (1960).

⁶I. Maartense, *Phys. Rev.* **188**, 924 (1969).

⁷D. C. Price *et al.* (unpublished).

⁸N. Y. Ikornikova, *Kristallografiya* **6**, 745 (1961) [*Sov. Phys. Cryst.* **6**, 594 (1962)].

⁹I. Maartense, *Rev. Sci. Instr.* **41**, 657 (1970).

¹⁰A. S. Borovik-Romanov, *Zh. Eksperim. i Teor. Fiz.* **36**, 766 (1959) [*Sov. Phys. JETP* **9**, 539 (1959)].

¹¹H. Bizette and B. Tsai, *Compt. Rend.* **238**, 1575 (1954).

¹²J. Smit and H. P. J. Wijn, *Ferrites* (Wiley, New York, 1959), p. 307.

¹³H. C. Meijer, L. M. W. A. Pimmelaar, S. R. Brouwer, and J. van den Handel, *Physica* **46**, 279 (1970).

¹⁴S. Iida and A. Tasaki, in *Proceedings of the International Conference on Magnetism, Nottingham, 1964* (The Institute of Physics and The Physical Society, London, 1964), p. 583.

¹⁵I. Maartense, *Solid State Commun.* **9**, 2071 (1971).

¹⁶K. N. Woods and M. E. Fine, *J. Appl. Phys.* **40**, 3425 (1969).

¹⁷H. N. Ok, *Phys. Rev.* **181**, 563 (1969).

¹⁸G. Cinader, *Phys. Rev.* **155**, 453 (1967); I. S. Jacobs, R. A. Beyerlein, S. Foner, and J. P. Remeika, *Intern. J. Magnetism* **1**, 193 (1971).

¹⁹T. Nagamiya, K. Yosida, and R. Kubo, *Advan. Phys.* **4**, 1 (1955).

²⁰P. L. Richards, *J. Appl. Phys.* **35**, 850 (1964).

²¹H. N. Ok, *Phys. Rev.* **185**, 472 (1969); D. W. Forester and N. C. Koon, *J. Appl. Phys.* **40**, 1316 (1969).

²²G. K. Wertheim, H. J. Guggenheim, M. Butler, and V. Jaccarino, *Phys. Rev.* **178**, 804 (1969).

²³L. F. Johnson, R. E. Dietz, and H. J. Guggenheim [*Phys. Rev. Letters* **17**, 13 (1966)] have studied quenching by Ni²⁺ impurities in ordered Mn²⁺ salts.